Desalination and Water Treatment
www.deswater.com

doi:10.5004/dwt.2019.24136

159 (2019) 346–355
August

Comparative assessment of the decolorization of aqueous bromophenol blue using Fe nanoparticles and Fe-Ni bimetallic nanoparticles

Raheeq Naser, Talal Shahwan*

Chemistry Department, Birzeit University, Ramallah, Palestinian Authority, email: raheeqnaser93@gmail.com (R. Naser), tshahwan@birzeit.edu (T. Shahwan)

Received 2 December 2018; Accepted 20 March 2019

ABSTRACT

Iron nanoparticles (Fe NPs) and bimetallic iron-nickel nanoparticles (Fe-Ni NPs) were synthesized by liquid phase reduction method, and were characterized using XRD, XPS, SEM and TEM techniques. A comparative study was performed to assess the efficiency of Fe and Fe-Ni NPs in the removal of bromophenol blue (BPB) dye from aqueous media. The effects of pH, time, initial dye concentration, and temperature on the removal process were investigated. The results showed that the highest dye removal is obtained at pH of 4.0. The removal of BPB follows a pseudo second order rate kinetics, with the dye removal by Fe NPs being faster than that achieved using Fe-Ni NPs, and the maximum sorption capacities being 1667 and 213 mg/g, respectively. Equilibrium constant (K) values were calculated using a modified form of the linear isotherm, and the K values at 298 K were 64416 and 11901 mL/g for Fe and Fe-Ni NPs, respectively. The removal of BPB by Fe NPs and Fe-Ni NPs was exothermic with ΔH° values being –35.8 and –51.9 kJ/mol, respectively. Entropy of the system decreased in both cases, and the corresponding values were –28.2 and –96.3 J/mol·K for Fe and Fe-Ni NPs, respectively.

Keywords: Fe nanoparticles; Fe-Ni nanoparticles; Bromophenol blue; Decolorization

1. Introduction

Environmental pollution is rapidly increasing and threatening the main environmental components; water, air and soil [1]. The global textile and clothing industry is very huge and produces large volumes of wastewater, which is often rich in colors and contains residues of reactive dyes [2]. The existing treatment methods are not effective enough to degrade textile dyes. The discharge of inadequately treated textile wastewater is considered a major environmental concern [3].

Bromophenol blue (BPB) is an acid dye, which is used as a color marker to monitor the process of agarose gel electrophoresis, polyacrylamide gel electrophoresis, coloring proteins in paper electrophoresis, and is also a pH indicator. This dye is widely used as an industrial dye for foods, drugs, cosmetics, textiles, printing inks and laboratory indicators [4]. The structure of the dye is shown in Fig. 1 [5].

*Corresponding author.

Various methods have been traditionally used for the removal of dye pollutants from wastewater, such as reverse osmosis, electrochemical coagulation, nano filtration, adsorption, and others [6]. Iron and iron based-nanoparticles have been widely proposed as effective materials for the removal of organic and inorganic aqueous pollutants such as organic dyes, chlorinated organic compounds and heavy metals [7]. The efficiency of iron nanoparticles is mainly due to the low oxidation-reduction potential and high surface area. In addition, it has been widely considered as an environmental friendly material [8].

Individual nZVI particles possess a spherical shape, with a core-shell structure. The core is composed of zero-valent iron Fe(0), which can act as an electron donor in redox reactions. The shell is composed of iron oxide and iron oxyhydroxide groups, which can take part in the uptake of pollutants form aqueous media. The nZVI material has a chain-like structure, which results from the strong magnetic forces among the individual particles [9]. Iron nanoparticles can also serve as a coagulant for various anions in ground-

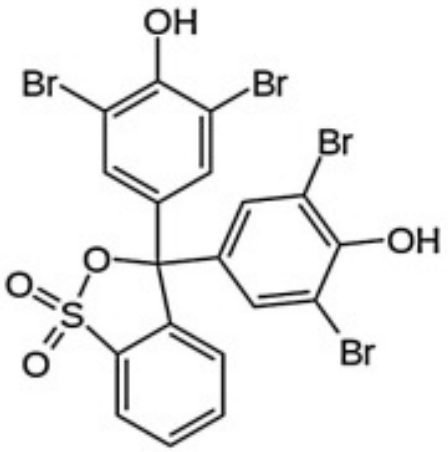

Fig. 1. Bromophenol blue structure.

water through the hydrolysis of Fe(II). The interfacial reactions of Fe (dissolution, adsorption, redox reaction, and precipitation) can occur simultaneously or sequentially on the surface of the nanoparticles during the decontamination process [10].

Bimetallic nanoparticles consist of two different metal elements synthesized with nanosize. Adding the second metal is reported to improve the catalytic properties of the original single metal [11]. The search for bimetallic nanoparticles containing iron is motivated by some of the limitations in the application of iron nanoparticles, originating primarily from its agglomeration in aqueous media, which can reach micrometer size [12]. Fe-Ni bimetallic nanoparticles has been widely synthesized and used in the removal of organic pollutants and dye stuff [13,14]. The catalytic properties of nickel are thought to stimulate the formation of atomic hydrogen or hydride on the surface, and enhance the electronic properties of the iron, thus expediting the reductive pathways of the dechlorination reactions [15].

Different studies are reported in literature about the removal of aqueous BPB. In one of those BPB was removed from water using activated charcoal as adsorbent material [5]. In another study, α-chitin nanoparticles were tested for the removal of BPB [16]. A polymer-clay composite consisting of kaolinite clay crosslinked with polyacrylamide co-acrylic was also studied as an adsorbent material of BPB [17]. It was also reported that TiO_2 could be used effectively to decolorize BPB under UV irradiation [18]. Furthermore, certain types of nanomaterials have been also reported in literature as possible choices for the removal of BPB such as Fe_2O_3–ZnO–$ZnFe_2O_4$/C nanocomposite and CuO-nano-clinoptilolite [19,20]. Our literature review did not, however, yield results about the removal of BPB by either Fe NPs or bimetallic Fe-Ni NPs, and to our knowledge this work is the first of its kind for BPB dye.

This study focuses first on the synthesis and characterization of Fe NPs and Fe-Ni NPs, and then using these materials in the removal of BPB from aqueous solution. The prepared materials were characterized using scanning electron microscopy (SEM), transmission electron microscopy (TEM), X-ray powder diffraction (XRD), and X-ray photoelectron spectroscopy (XPS). The BPB concentration was monitored using UV-visible spectrophotometry. The investigated experimental parameters included pH, contact time, dye initial concentration, and temperature.

2. Experimental

2.1. Chemicals and reagents

Throughout this study the following chemicals were used without further purification; ferrous sulfate heptahydrate $FeSO_4{\cdot}7H_2O$ (Aldrich 7782-63), nickel chloride hexahydrate $NiCl_2{\cdot}6H_2O$ (Aldrich 7791-20), sodium borohydride, $NaBH_4$, (Merck 8.06373), absolute ethanol (J.T. Baker 8006), bromophenol blue $C_{19}H_{10}Br_4O_5S$ (95%) (Aldrich 61698), potassium dihydrogen phosphate KH_2PO_4 (Aldrich 45369), and potassium hydrogen phthalate (KHP; $C_8H_5KO_4$) (Merck 545-K764274). All aqueous solutions were prepared using deionized water.

2.2. Synthesis of Fe NPs, Ni NPs, and Fe-Ni NPs

Iron nanoparticles and iron-nickel bimetallic nanoparticles were prepared using liquid phase reduction method with sodium borohydride as the reducing agent, in accordance with procedures reported in previous publications [21,22].

In order to prepare Fe NPs, 5.34 g of $FeCl_2{\cdot}4H_2O$ was dissolved in 25.0 mL 4:1 (ethanol: water) solution in each batch, and was kept under magnetic stirring conditions for 15 min. The $NaBH_4$ solution was prepared separately by dissolving 2.54 g in 70.0 mL of water. Then, the borohydride solution was added to the iron solution using a burette at a constant addition rate of about 0.5 mL s^{-1} under continuous magnetic stirring conditions. During the addition of the borohydride solution, the iron solution color converted from brown to black and H_2 gas evolution was observed. A sharp rise in pH occurred, indicating successful reduction of Fe^{2+} to Fe^0 according to the following chemical equation:

$$Fe^{2+} + 2BH_4^- + 6H_2O \rightarrow Fe^0 + 2B(OH)_3 + 7H_{2(g)}\uparrow$$

The solution of Fe NPs was kept under stirring condition for another 15 min, and vacuum filtration was used to separate the produced Fe NPs. While still on suction filter, the black Fe NPs powder was washed with absolute ethanol three times. Finally, the obtained Fe NPs sample was dried in the oven at 90°C for 6 h, and was stored for future use.

The same procedure was used to synthesize Ni NPs. For this purpose, 6.45 g of $NiCl_2{\cdot}6H_2O$ were dissolved in 25.0 mL 4:1 (ethanol: water) solution, and were kept for 15 min. under magnetic stirring condition. The $NaBH_4$ solution was prepared separately by dissolving 5.67 g in 70.0 mL of water. Then, the borohydride solution was added to the nickel solution using a burette at a constant addition rate of about 0.5 mL s^{-1} under continuous magnetic stirring condition. The solution was finally filtered, washed and dried, and stored for future use.

The Fe-Ni NPs samples were prepared by dissolving 3.0750 g $FeSO_4{\cdot}7H_2O$ and 0.7500 g $NiCl_2{\cdot}6H_2O$ in 25.0 mL of a 4:1 (ethanol: water) solution, and was kept for 15 min. under magnetic stirring condition. The $NaBH_4$ solution was

prepared separately by dissolving 2.54 g in 70.0 mL of water. Then, the borohydride solution was added to the Fe-Ni solution using a burette at a constant rate of approximately 0.5 mL s^{-1} under continuous magnetic stirring condition. The mixture was then kept under continuous stirring for another 15 min. Vacuum filtration was used to separate the produced NPs, and while still on suction filter, the nanoparticle powder was washed with absolute ethanol three times. Finally, the resulting Fe-Ni NPs sample was dried in the oven at 90°C for 6 h, and was stored for future use.

2.3. Dye removal experiments

Throughout this study, all of the solutions were prepared in potassium hydrogen phthalate (KHP) buffer solution (pH = 4.0). This solution was prepared in accordance with a procedure reported in literature [5]. For this purpose, 10.21 g of KHP salt and 1.0 mL of 0.10 M HCl were dissolved in 1.0 L deionized water using a volumetric flask. A stock solution of bromophenol blue (BPB) at a concentration of 100 mg/L was prepared by dissolving exactly 26.3 mg dye in 250 ml KHP buffer solution (at pH = 4.0). Further analytical dilutions were made when needed using volumetric pipettes. A linear calibration curve was constructed for BPB in the concentration range of 1.0–10.0 mg/L. The calibration curve was obtained by measuring the UV-Visible absorbance at λ_{max} (590 nm) of the dye using Varian Cary 50 UV-Visible spectrophotometer.

The dye removal experiments where performed using freshly prepared dye solutions obtained by serial dilutions from the stock solution. Following the decolorization experiments, the absorbance was measured directly for solution aliquots, and in some cases further dilutions were made to account for high absorbance. All the experiments were performed under atmospheric pressure using polypropylene falcon tubes under shaking conditions. These tubes are appropriate for shaking in the water bath, are thermally stable, and their volumes are suitable for the solution volumes used in the experiments.

2.3.1. Effect of pH

The pH was adjusted to different values (4.0, 6.0, and 8.0) by using KHP or KH_2PO_4 buffers, in which the BPB powder was dissolved. The buffer solutions were prepared by dissolving the appropriate weights of KHP or KH_2PO_4. The pH was adjusted to the specified values by further additions of 0.1 M HCl or 0.1 M NaOH, then deionized water was added to fill up to 1.0 liter volume.

2.3.2. Dye removal kinetics

Prior to performing the kinetic experiments, the removal of BPB dye was tested using three different doses of Fe NPs; 0.010, 0.0050, and 0.0010 g. The removal of the dye by Fe NPs was very fast and highly dependent on the amount of Fe NPs. The results showed that the removal of BPB was almost complete after 1 min. of contact when 0.010 g of Fe NPs was used. Hence, in order to be able to follow the kinetic progress of the removal process, the related experiments were conducted at a dose of 0.0010 g Fe NPs.

On the other hand, in the case of Fe-Ni NPs and Ni NPs, 0.0100 g dose was used due to low removal efficiency at a 0.0010 g amount.

The three adsorbents (Fe, Ni, Fe-Ni NPs) were added separately to 25.0 mL of 100.0 mg/L BPB dye solutions. The mixtures were kept in contact for different time periods in different falcon tubes. Subsequently, the dye solutions were separated from the adsorbents by filtration, and were analyzed using UV-Vis spectrophotometry.

2.3.3. Effect of initial dye concentration and temperature

In these experiments, a fixed weight (0.0100 g) of Fe NPs and Fe-Ni NPs was mixed separately with 25.0 mL portions of BPB dye at initial concentrations of 20.0, 40.0, 60.0, 80.0 and 100.0 mg/L, and was kept in contact for 1 h at 298 K. The dye was then separated from the adsorbent by filtration. In order to test the effect of temperature, the same experiments were repeated under the same conditions by adjusting the thermostat water bath at 323 K.

2.4. Characterization techniques

The dye concentrations were measured using a Varian Cary 50 UV-Visible Spectrophotometer. The spectrophotometer operates on dual beam using a Czerny-Turner monochromator at 190–1100 nm wavelength range with approximately 1.5 nm fixed spectral bandwidth. The light source consists of full spectrum Xe pulse lamp, and has dual Si diode detectors. The spectrophotometer was used to obtain calibration curves for BPB in the concentration range of 1.0–10.0 mg L^{-1} respectively, at λ_{max} of 590 nm.

Powder XRD data were collected on a STOE Stadi P diffractometer, located at Helmholtz Institute Ulm, Germany. The source consists of Cu Kα1 (λ = 1.54 Å) radiation at 40 kV/ 40 mA. The samples were scanned from 2θ of 5 up to 80°.

The morphology of the nanoparticles was studied using Scanning Electron Microscopy (SEM). The images were recorded using a Hitachi, S-5200 field-emission scanning electron microscope, Hitachi, Tokyo, Japan located at University of Ulm, electron microscopy department, Germany. The accelerating voltage is 10 kV, and the images were taken with the secondary electron detector.

Transmission Electron Microscopy (TEM) images were recorded with a Jeol-1400 instrument, located at University of Ulm, electron microscopy department, Germany. The images were taken under an accelerating voltage of 120 kV, bright field signals. After preparation, the samples were placed on a copper grid and fixed on the device holder, and the parameters were adjusted to obtain clear images. During SEM and TEM analysis, the samples were dispersed in ethanol for few minutes using a sonicator, then one drop from the suspension was placed on a copper grid which then was fixed on a special holder and placed in the instrument.

X-ray photoelectron spectroscopy (XPS, Multiprobe, Omicron Nanotechnology) was performed in a multi-technique UHV instrument using a monochromatic Al Kα X-ray source (1486.7 eV, 270 W), and the chamber pressure was 5×10^{-10} mbar. The equipment is located at Physics department in Bielefeld University, Germany. The sample was

dispersed in ethanol using ultrasonic shaker path, then few drops of the suspension were placed on piece of silicon/silicon oxide substrate. The analysis of the XP spectra was carried out using CasaXPS software, and a Shirley background subtraction procedure was employed.

3. Results and discussion

3.1. Characterization of the nanoparticles materials

3.1.1. Characterization of Fe NPs

The structure of Fe NPs was characterized using XRD. Fig. 2a shows the basic reflection of metallic iron (110) at 2θ = 44.9°. The reflections of iron oxides are very weak, indicating that nZVI is the major component of the Fe NPs material.

Typical SEM and TEM images of Fe NPs are shown in Fig. 3. The morphology of the iron sample matches with the results reported in earlier publications [e.g. 23–25]. As shown in the SEM and TEM images, the diameter of individual Fe nanoparticles is in the range (40–80) nm, and it is aggregated into chain-like structures; a typical behavior attributed to the magnetic attractive forces between the individual iron particles. The dark color in the TEM image is attributed to the presence of metallic iron, and the lighter regions refer to the oxidized iron on the surface shells. It is well known that the individual Fe nanoparticles possess a core-shell structure in which the core is composed of Fe in its zero-valence state, while the shell contains iron oxides and oxyhydroxides [26].

A wide XPS survey, in addition to Fe 2p peak spectrum, is shown in Fig. 4. The photoelectron peak at the binding energy of 285.5 eV corresponds to C 1s photoelectrons arising from adventitious sources. The O 1s feature appearing at 533 eV originates from O^{2-} in metal oxides. The Fe 2p features at 727 eV and 713 eV are attributed to the binding energies of Fe $2p_{1/2}$ and $2p_{3/2,}$ respectively. The satellite peaks are observed around 720 and 730 eV. These features indicate that the shell in Fe NPs is composed mainly of iron oxides and iron oxyhydroxides. The weak feature appearing at 707 eV arises from Fe $2p_{3/2}$attributed to zero-valent iron (Fe^0). The results reflect the core-shell nature of nZVI [27].

3.1.2. Characterization of Fe-Ni NPs

The XRD pattern of a sample of Fe-Ni NPs is shown in Fig. 2b. The broad peak centered at 2θ of 43–45 seems

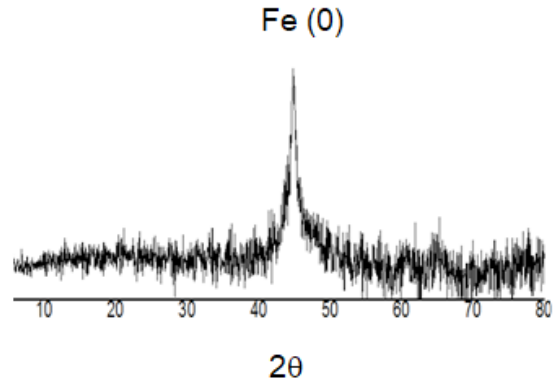

(a)

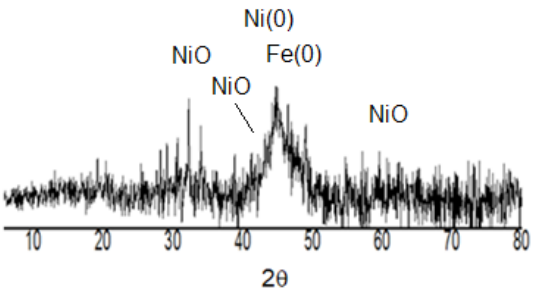

(b)

Fig. 2. a) XRD pattern showing the basic reflection of metallic iron in Fe NPs, b) XRD pattern showing the basic reflections of metallic Fe and Ni in Fe-Ni NPs.

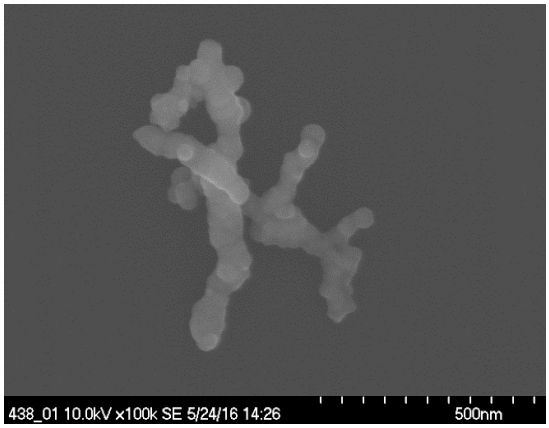

(a)

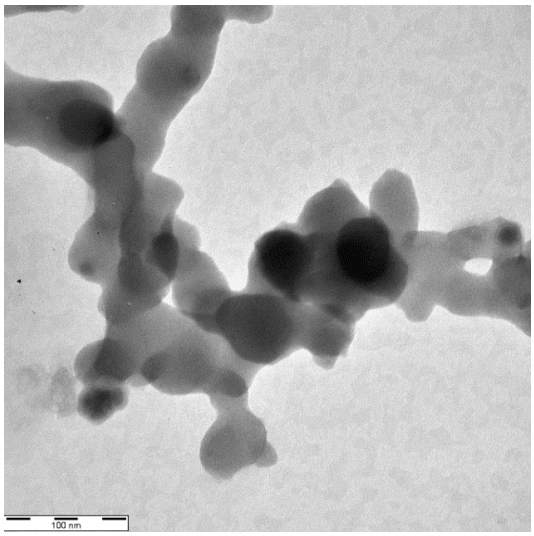

(b)

Fig. 3. Typical a) SEM image, b) TEM image, of Fe NPs.

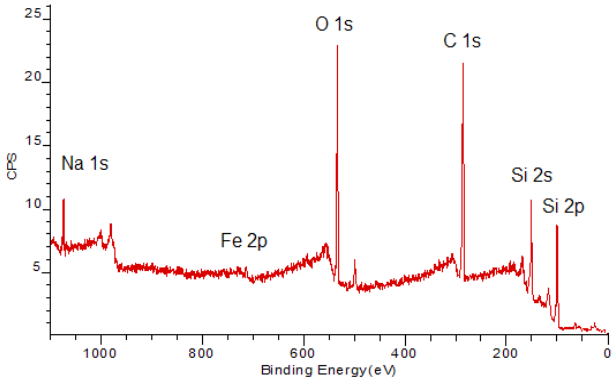

(a)

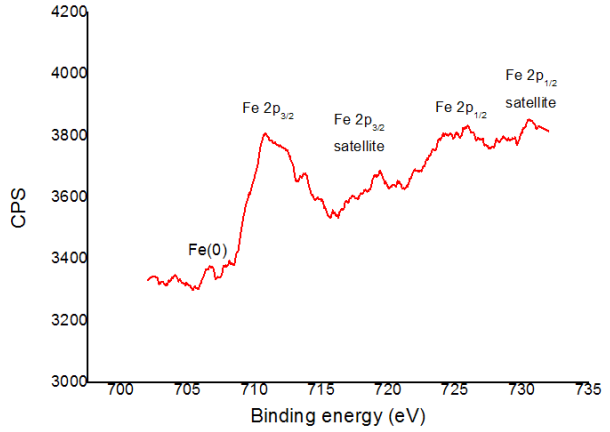

(b)

Fig. 4. a) Wide XPS spectrum, b) Fe 2p features, of Fe NPs.

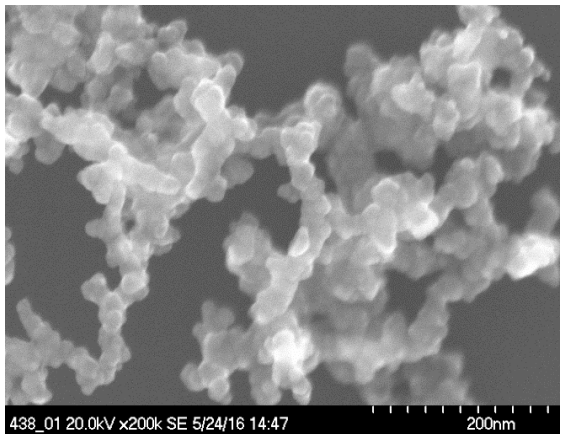

(a)

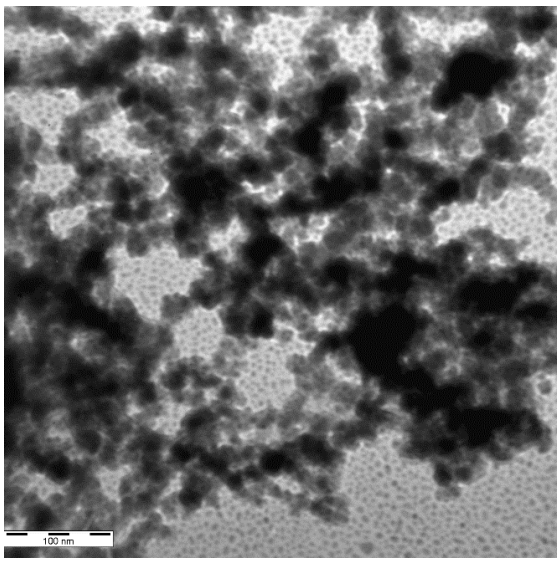

(b)

Fig. 5. Typical a) SEM, b) TEM images of Fe-Ni bimetallic NPs.

to correspond to the overlap between metallic Ni(111) major reflection (44.5°) and metallic Fe (110) major reflection (44.9°) [28,29]. The XRD pattern contains also the basic reflections of NiO; (200), (111), and (220). The peaks appear to be broad and the corresponding intensities are low indicating that the material is mostly amorphous.

The SEM and TEM analysis of Fe-Ni bimetallic nanoparticles indicated aggregation due to the magnetic properties of Fe and Ni metals leading to the well known chain-like structure, as shown in Fig. 5 (a,b). This is in line with earlier reports about this material [15]. The particle size appears to be smaller than that of Fe NPs. In order to check the particle size, Helium ion microscope (HIM) analysis was performed. According to the results, the diameter of individual nanoparticles is approximatly 40–50 nm, which is roughly half of that observed for Fe NPs.

The wide XPS survey in Fig. 6a shows the elements in the Fe-Ni. The Fe 2p peak in Fig. 6b is similar to that in pure Fe NPs, and indicates the presence of iron oxides and hydroxide in addition to zero-valent iron. The Ni $2p_{3/2}$ and Ni $2p_{1/2}$ doublet in the Ni 2p peak are attributed to nickel oxide and hydroxide [30]. While the XPS features corresponding to Fe 2p in Fe-Ni NPs show the presence of iron in its zero-valent state (around 707 eV), the feature corresponding to zero-valent nickel appears very weak. On the overall, as reflected by the colour contrast, the extent of oxidation in Fe-Ni NPs seems to be more pronounced compared with Fe NPs. This is in line with the XRD characterization results which showed significant formation of NiO in addition to metallic Fe and Ni.

3.2. *Effect of pH*

The effect of pH on the removal of BPB by Fe and Fe-Ni NPs was investigated using a buffer system adjusted at values of 4.0, 6.0 and 8.0. This "intermediate" pH range was chosen in order to avoid excessive acidic or basic media which could cause, respectively, dissolution of iron NPs, or precipitation of iron hydroxide species. The removal process was very efficient at pH 4, as given by the data in the subsequent sections, but the extent of removal was negligible at the higher pH values. As known, BPB is an acid

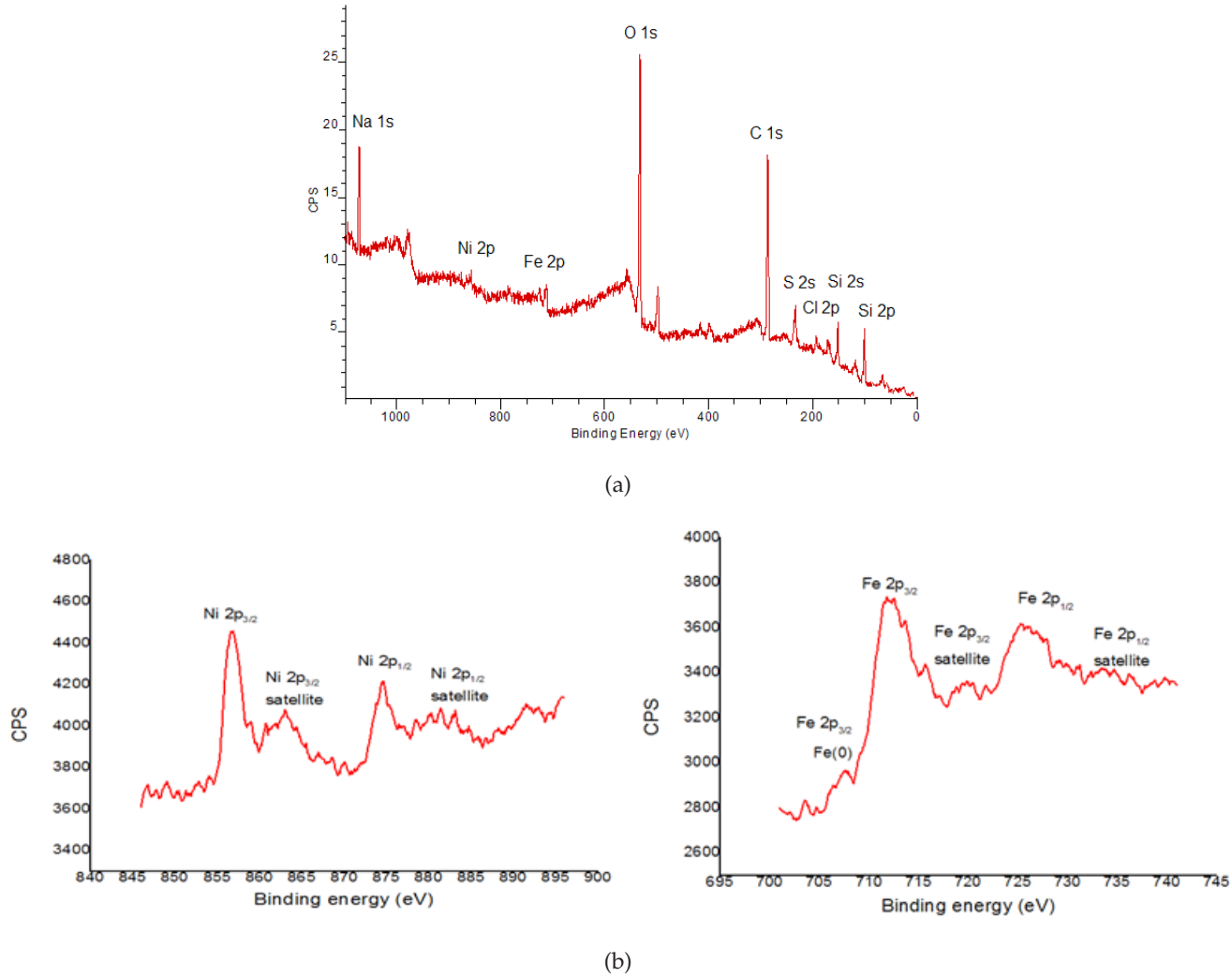

Fig. 6. a) Wide XPS spectrum, b) Ni 2p and Fe 2p features, of Fe-Ni NPs.

dye which carries a slight negative charge at moderate pH. Hence, the dye is more active in surface bonding at low pH values. As such, its extent of removal is expected to decrease as pH increases due to the development of negative surface charge on the sorbent at high pH values. In addition, low pH values cause enhancement in nZVI reactivity, which is induced by the acceleration of iron corrosion and dissolution of the passivated layers on the nZVI surface. Moreover, at high pH values, nZVI reactivity can be lowered due to the precipitation of ferrous hydroxide on the nZVI surfaces, leading to the inhibition of electron transfer from the Fe(0) core to the outermost oxide surface [10].

Based on these results, the subsequent experiments were performed at pH of 4.0.

3.3. Effect of time

The variation of the BPB liquid concentration with time is plotted in Fig. 7 for Fe and Fe-Ni NPs. In both cases, the dye removal is seen to approach equilibrium in less than an hour. For the sake of comparison, similar experiments were also performed using pure Ni NPs. The dye removal by Ni NPs was very limited and did not exceed 30% even after 1 hour of contact between the dye solution and Ni NPs. This is indicative that Ni^0 is less effective that Fe^0 in dye removal.

Although the removal mechanism may involve reductive degradation of BPB dye, adsorption of the dye molecules on the nanoparticles surface is essential as a preliminary step. The concentration of the adsorbed dye can be linked to its concentration in solution through the mass balance equation given by:

$$Q = (C_o - C)\frac{V}{m} \quad (1)$$

where Q is the solute concentration on the solid (mg g^{-1}) at a given time, C_0 is the initial solute concentration (mg L^{-1}), C is the solute concentration at a given time (mg L^{-1}), m is the mass of the sorbent (g), and V is the solution volume (L).

The kinetic data was tested by a pseudo first order equation (Lagergren's equation), and by two pseudo second order rate equation (suggested by Ho [31] and by Shahwan [32]). These equations are, respectively, given as:

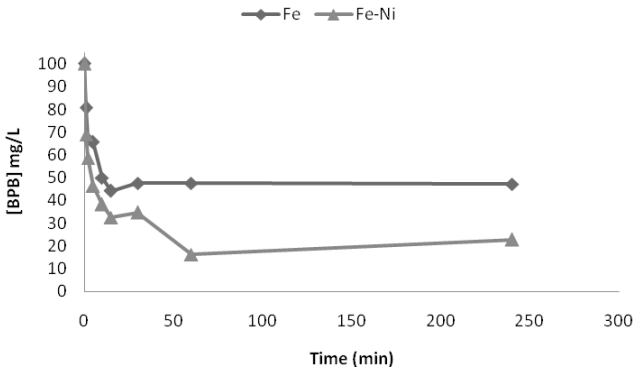

Fig. 7. Variation of dye concentration with time for Fe and Fe-Ni NPs.

$$\ln\left(Q_e - Q\right) = \ln Q_e - kt \tag{2}$$

$$Q = \frac{Q_e^2 kt}{1 + Q_e kt} \tag{3}$$

$$Q = \frac{Q_m C_o kt}{C_o kt + 1} \tag{4}$$

Eqs. (3) and (4) can be linearized as:

$$\frac{t}{Q} = \frac{1}{Q_e^2 k} + \frac{1}{Q_e} t \tag{5}$$

$$\frac{t}{Q} = \frac{1}{Q_m C_o k} + \frac{1}{Q_m} t \tag{6}$$

In the two equations, the dependent and independent variables are the same, however, the slope and intercepts are different. In both cases, k is the rate constant, though the unit is different. Q_e in Eq. (5) is the equilibrium amount of the sorbed dye, and Q_m in Eq. (6) is the maximum amount of solute that would be sorbed if the sorption reaction goes to completion (equals to V/m multiplied by C_0).

In constructing the linear plots, the data points corresponding to the pre-equilibrium stages were used. The linear correlation of the kinetic data with Lagergren's equation [Eq. (2)] was poor for both types of nanomaterials. On the other hand, the pseudo second order equations provided adequate description of the kinetic data, and the coefficients of determination (r^2) were 0.9738 and 0.9843 for Fe NPs and Fe-Ni NPs, respectively.

The linear fits of the kinetic data of BPB removal by Fe NPs and Fe-Ni NPs are shown in Fig. 8. The rate constants calculated using Eq. (5) for the dye removal by Fe NPs and Fe-Ni NPs were 0.000212 g·mg^{-1}·min^{-1} and 0.001381 g·mg^{-1}·min^{-1}. On the other hand, the corresponding rate constants obtained using Eq. (6) were 0.00353 L·mg^{-1}·min^{-1} and 0.00294 L·mg^{-1}·min^{-1}.

In order to compare the correlation of the data with Eqs. (5) and (6), the Chi test was performed. The test is based on comparing the experimental data with the data predicted by each of the two Eqs. (5) and (6). For this purpose the following formula was used [31]:

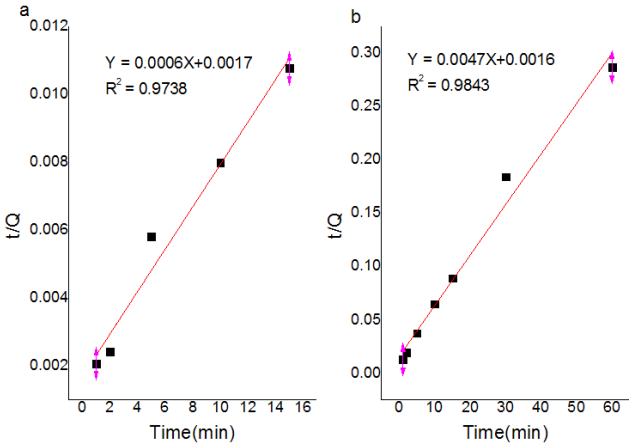

Fig. 8. Pseudo second order linear fits for the removal of BPB by: (a) Fe NPs (b) Fe-Ni NPs.

$$\chi^2 = \sum_{1}^{n} \frac{\left(Q_{\exp} - Q_{model}\right)^2}{Q_{model}} \tag{7}$$

A smaller value of χ^2 means that the difference between experimental and predicted values is smaller, and vice versa. The calculated values of χ^2 for Fe NPs obtained from the linear regressions of Eqs. (5) and (6) were, respectively, 1648 and 217, whereas the χ^2 values for Fe-Ni NPs case were 31.4 for both equations. These results indicate that the Q values predicted by Eq. (6) are closer to the experimental values. The rate constants obtained by Eq. (6) indicate faster removal of BPB by Fe NPs compared to Fe NPs.

3.4. Effect of initial dye concentration at 298 K

The effect of initial BPB concentration on the extent of the dye removal was investigated for both of Fe NPs and Fe-Ni NPs at the initial dye concentrations of 20.0, 40.0, 60.0, 80.0 and 100.0 mg L^{-1}. The time of contact was kept at 1 h, and the experiments were conducted at 298 K. The obtained results, given in Table 1, confirm that Fe NPs are superior in BPB removal at all studied concentrations.

The obtained data was tested using Langmuir and Freundlich isotherms, but the linear correlation was poor in both cases. Hence, and in order to elucidate the partitioning constant of BPB among liquid and solid phases, a new approach was used. As shown below, the approach is based on a combination of the linear isotherm with the mass balance equation. This method has been recently reported in one of our studies for the removal of methylene blue by Fe NPs and provided adequate correlation with the experimental data [33].

The linear isotherm is given by the relation:

$$Q = KC \tag{8}$$

K stands here for the distribution ratio of the solute between the solid and liquid phases. Using the mass balance equation for a single stage batch process (given in Eq. (1)) the linear isotherm becomes:

Table 1
The calculated Q values of BPB on the two NPs types at various BPB initial concentrations.

	Q (mg/g) at 298 K		Q (mg/g) at 323 K	
C_0 (mg/L)	Fe NPs	Fe-Ni NPs	Fe NPs	Fe-Ni NPs
20	47	39	45	23
40	96	82	91	48
60	141	116	138	73
80	194	159	181	100
100	243	218	219	119

$$Q = K(C_0 - \frac{Q \cdot m}{V} \quad (9)$$

Rearranging;

$$Q = \frac{K}{1 + \frac{K \cdot m}{V}} C_0 \quad (10)$$

Since K, m, and V are all constants, the equation can be written as:

$$Q = K' C_0 \quad (11)$$

where $K' = \frac{K}{1 + \frac{K \cdot m}{V}}$.

K' can be obtained from the slope of Q vs C_0 linear plots, and used to calculate the apparent equilibrium constant, K:

$$K = \frac{K'}{1 - \frac{K' \cdot m}{V}} \quad (12)$$

The K values are then used to calculate standard Gibbs energy change (ΔG°) values using the well-known thermodynamic relation, which is valid under equilibrium condition:

$$\Delta G^0 = -RT \ln K \quad (13)$$

The data in Table 1 were fitted to Eq. (11), as shown in Fig. 9, and the slope of each figure was used to calculate K' and K values, which were then used to obtain ΔG° values, as provided in Table 2.

The table indicates clearly that Fe NPs are more effective in BPB removal than Fe-Ni NPs, as reflected by the higher K values. In all cases, the sorption reactions favor the products over the reactants, as indicated by the negative ΔG° values.

3.5. Effect of initial dye concentration at 323 K

In order to reveal the effect of temperature on the extent of dye removal, the effect of initial dye concentration was also studied at 323 K. The removal experiments were performed using Fe and Fe-Ni nanoparticles at the initial dye concentrations of 20, 40, 60, 80.0 and 100.0 mg/L, and the time of contact was 1 h. The results are given in Table 1.

In order to calculate the equilibrium constants at 323 K, the experimental data were fitted using Eq. (11), as shown in Fig. 9, and the slope of each figure was used to calculate K' and K values. The obtained K values were used to calculate the standard enthalpy change, ΔH°, utilizing the well-known van't Hoff equation, which has been widely applied before for this purpose [e.g. 5,33]:

Table 2
Values of coefficient of determination (R^2), K', K, and ΔG^0 obtained for sorption of BPB on Fe NPs and Fe-Ni NPs at 298 K.

	Fe NPs	Fe-Ni NPs
Slope	2.4066	2.0660
R^2	0.9992	0.9876
K'(ml/g)	2406	2066
K (ml/g)	64416	11901
ΔG^0 (kJ/mol)	–27.4	–23.2

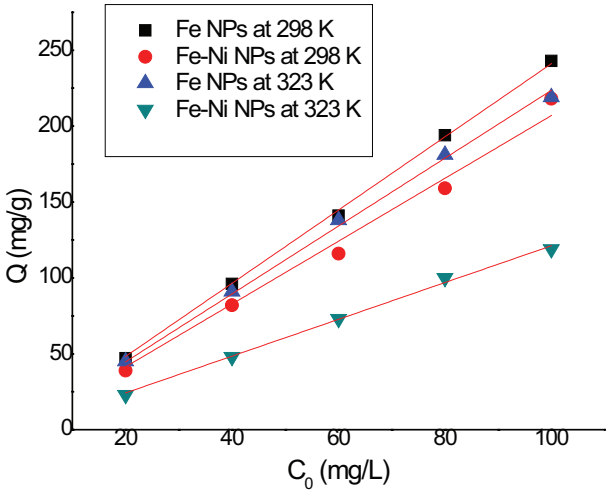

Fig. 9. Variation of Q with C_0 for BPB using Fe NPs and Fe-Ni NPs at 298 K and 323 K.

$$\ln \frac{K_2}{K_1} = -\frac{\Delta H^o}{R}\left(\frac{1}{T_2} - \frac{1}{T_1}\right) \quad (14)$$

The standard entropy change, ΔS°, of sorption was calculated using the following equation:

$$\Delta S° = \frac{\Delta H° - \Delta G°}{T} \quad (15)$$

The obtained values of ΔG°, ΔH°, and ΔS° are provided in Tables 3 and 4.

The values of enthalpy change are negative for BPB removal by both of Fe and Fe-Ni, indicating exothermic behavior. In both cases, negative entropy changes of the system are obtained. The negative standard Gibbs energy changes show that the reaction distinctly favors the products over the reactants.

The exothermic behavior and the negative entropy changes of BPB sorption on both nanomaterials can be attributed to the relatively low hydration energies of the solute, which leads to high chemical potential of the BPB molecules in the solution. In such a case, the fixation of

Table 3
Values of coefficient of determination (R^2), K′, K, and ΔG° obtained for sorption of BPB on Fe NPs and Fe-Ni NPs at 323 K.

	Fe NPs	Fe-Ni NPs
Slope	2.2343	1.2109
R^2	0.9975	0.9969
K' (ml/g)	2234	1211
K (ml/g)	20996	2349
ΔG° (kJ/mol)	–26.7	–20.8

Table 4
The calculated values of ΔH° and ΔS° associated with removal of BPB from aqueous solutions containing Fe NPs and Fe-Ni NPs.

Sample	ΔH° (kJ/mol)	ΔS° (J/mol·K)
Fe NPs	–35.8	–28.2
Fe-Ni NPs	–51.9	–96.3

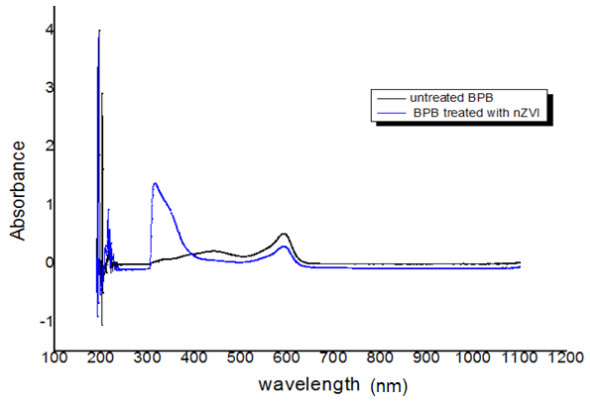

Fig. 10. UV-Vis spectra of BPB before and after treatment with Fe NPs.

the solute on the solid surface will be driven by intrinsic enthalpy changes (exothermic), with small contribution from enthalpy of dehydration (endothermic). As such the resulting enthalpy change is exothermic. The overall sorption process causes an increase in the order of the system, yielding a negative entropy change. In the specific case of BPB, this can be rationalized based on the fact that the dye molecules are nearly charge less, with a relatively large molecular size. Hence, BPB is not expected to have strong hydration energies in water, as it is the case with charged and small molecules.

Finally, the U-Vis spectra of BPB solutions obtained at the end of the removal process showed the disappearance of the dye peaks at 590 nm and 440 nm, and the appearance of a new intense peak at 317 nm. Fig. 10 provides two typical spectra. This result could be considered as an indication of the degradation of the BPB during the removal process by nanoparticles materials. This topic and the identification of the degradation products needs further investigation in a separate study.

4. Conclusions

Fe NPs and Fe-Ni NPs can readily be prepared by liquid phase reduction using sodium borohydride as a reducing agent. Fe-Ni NPs were observed to be smaller in size than Fe NPs. Both of the materials possess chain-like morphology. Comparing the efficiency of Fe and Fe-Ni NPs in removing BPB dye from water, the following conclusions can be summarized:

- In terms of the extent of dye removal, the efficiency of BPB removal using Fe NPs was higher than that obtained using Fe-Ni NPs.
- Fe NPs remove aqueous BPB faster than Fe-Ni NPs, and the process in both cases can be described by pseudo second order kinetics.
- Apparent equilibrium constants can be calculated using a modified form of the linear isotherm, in which the initial concentration is the dependent variable.
- The removal of BPB is an exothermic process in both cases, and leads to decrease in the entropy of the system.
- Future studies are needed to investigate the degradation products of the reaction. In addition, further experiments can be performed to comparatively test both materials as Fenton-like catalysts.

Acknowledgement

The chemicals used in this study were purchased from a research fund provided by Birzeit University (project no. 255162). The authors would like to thank Dr. Montaha Anjass at Ulm University for the help in SEM, TEM, and XRD characterization, and Prof. Armin Gölzhäuser and Dr. Yang Yangat Bielefeld University for the help in XPS characterization.

References

[1] I.S. Yunus, Harwin, A. Kurniawan, D. Adityawarman, A. Indarto, Nanotechnologies in water and air pollution treatment, Environ. Technol. Rev., 1 (2012) 136–148.
[2] A.K. Mehari, S. Gebremedhin, B. Ayele, Effect of Bahir Dar textile factory effluents on the water quality of the head waters Blue Nile Rivers, Ethiopia, Int. J. Anal. Chem. (2015).
[3] S.K. Raman, Textile dye degradation using nano zero valent iron: A review, J. Environ. Manage., 177 (2016) 341–355.
[4] R. Azmat, Z. Khalid, M. Haroon, K. Perveen, Spectral analysis of catalytic oxidation and degradation of bromophenol blue at low pH with potassium dichromate, Adv. Nat. Sci., 6 (2013) 38–43.
[5] M.J. Iqbal, M.N. Ashiq, Adsorption of dyes from aqueous solutions on activated charcoal, J. Hazard. Mater., 139 (2007) 57–66.
[6] V.K. Gupta, Suhas, Application of low-cost adsorbents for dye removal – A review, J. Environ. Manage., 90 (2009) 2313–2342.
[7] X. Li, W. Zhang, Iron nanoparticles: the core-shell structure and unique properties for Ni(II) sequestration, Langmiur, 22 (2006) 4638–4642.
[8] G. Bystrzejewska-piotrowska, J. Golimowski, P.L. Urban, Nanoparticles: their potential toxicity, waste and environmental management, Waste Manage., 29 (2009) 2587–2595.
[9] D. O'Carroll, B. Sleep, M. Krol, H. Boparai, C. Kocur, Nanoscale zero valent iron and bimetallic particles for contaminated site remediation, Adv. Water Res., 51 (2013) 104–122.

[10] S. Bae, K. Hanna, Reactivity of nanoscale zero-valent iron in unbuffered systems: effect of pH and Fe(II) dissolution, Environ. Sci. Technol., 49 (2015) 10536–10543.
[11] N. Toshima, T. Yonezawa, Bimetallic nanoparticles novel materials for chemical and physical applications, New J. Chem., (1998) 1179–1201.
[12] N. Efecan, T. Shahwan, A.E. Eroğlu, I. Lieberwirth, Characterization of the uptake of aqueous Ni^{2+} ions on nanoparticles of zero-valent iron (nZVI), Desalination, 249 (2009) 1048–1054.
[13] A.D. Bokare, R.C. Chikate, C.V. Rode, K.M. Paknikar, Iron-nickel bimetallic nanoparticles for reductive degradation of azo dye Orange G in aqueous solution, Appl. Catal. B, 79 (2008) 270–278.
[14] D.E. Meyer, K. Wood, L.G. Bachas, D. Bhattacharyya, Degradation of chlorinated organics by membrane-immobilized nanosized metals, Environ. Prog., 23 (2004) 232–242.
[15] Y. Tee, E. Grulke, D. Bhattacharyya, Role of Ni/Fe nanoparticle composition on the degradation of trichloroethylene from water, Ind. Eng. Chem. Res., 44 (2005) 7062–7070.
[16] S. Dhananasekaran, R. Palanivel, S. Pappu, Adsorption of methylene blue, bromophenol blue, and coomassie brilliant blue by α-chitin nanoparticles, J. Adv. Res., 7 (2016) 113–124.
[17] A.A. El-zahhar, N.S. Awwad, E.E. El-katori, Removal of bromophenol blue dye from industrial waste water by synthesizing polymer-clay composite, J. Mol. Liq., 199 (2014) 454–461.
[18] N. Bouanimba, R. Zouaghi, N. Laid, T. Sehili, Factors influencing the photocatalytic decolorization of bromophenol blue in aqueous solution with different types of TiO_2 as photocatalysts, Desalination, 275 (2011) 224–230.
[19] A. Mohammadzadeh, M. Ramezani, A.M. Ghaedi, Synthesis and characterization of Fe_2O_3–ZnO–$ZnFe_2O_4$/carbon nanocomposite and its application to removal of bromophenol blue dye using ultrasonic assisted method: Optimization by response surface methodology and genetic algorithm, J. Taiwan Inst. Chem. Eng., 59 (2016) 275–284.
[20] A. Nezamzadeh-Ejhieh, H. Zabihi-mobarakeh, Heterogeneous photodecolorization of mixture of methylene blue and bromophenol blue using CuO-nano-clinoptilolite, J. Ind. Eng. Chem., 20 (2014) 1421–1431.
[21] B. Schrick, J.L. Blough, A.D. Jones, T.E. Mallouk, Hydrodechlorination of trichloroethylene to hydrocarbons using bimetallic nickel-iron nanoparticles, Chem. Mater., 14 (2002) 5140–5147.
[22] D. Karabelli, S. Ünal, T. Shahwan, A.E. Eroğlu, Preparation and characterization of alumina-supported iron nanoparticles and its application for the removal of aqueous Cu^{2+} ions, Chem. Eng. J., 168 (2011) 979–984.
[23] M. Nairat, T. Shahwan, A.E. Eroglu, H. Fuchs, Incorporation of iron nanoparticles into clinoptilolite and its application for the removal of cationic and anionic dyes, J. Ind. Eng. Chem., 21 (2015) 1143–1151.
[24] O. Çelebi, Ç. Üzüm, T. Shahwan, H.N. Erten, A radiotracer study of the adsorption behavior of aqueous Ba^{2+} ions on nanoparticles of zero-valent iron, J. Hazard. Mater., 148 (2007) 761–767.
[25] Ç. Üzüm, T. Shahwan, A.E. Eroğlu, I. Lieberwirth, T.B. Scott, K.R. Hallam, Application of zero-valent iron nanoparticles for the removal of aqueous Co^{2+} ions under various experimental conditions, Chem. Eng. J., 144 (2008) 213–220.
[26] A. Liu, J. Liu, W. Zhang, Transformation and composition evolution of nanoscale zero valent iron (nZVI) synthesized by borohydride reduction in static water, Chemosphere, 119 (2015) 1068–1074.
[27] A.P. Grosvenor, B.A. Kobe, M.C. Biesinger, N.S. McIntyre, Investigation of multiplet splitting of Fe 2p XPS spectra and bonding in iron compounds, Surf. Interface Anal., 36 (2004) 1564–1574.
[28] S.H. Wu, D.H. Chen, Synthesis and characterization of nickel nanoparticles by hydrazine reduction in ethylene glycol, J. Colloid Interface Sci., 259 (2003) 282–286.
[29] D.H. Chen, C.H. Hsieh, Synthesis of nickel nanoparticles in aqueous cationic surfactant solutions, J. Mater. Chem., 12 (2002) 2412–2415.
[30] M.C. Biesinger, B.P. Payne, A.P. Grosvenor, L.W.M. Lau, A.R. Gerson, R. St. C. Smart, Resolving surface chemical states in XPS analysis of first row transition metals, oxides and hydroxides: Cr, Mn, Fe, Co and Ni, Appl. Surf. Sci., 257 (2011) 2717–2730.
[31] Y.-S. Ho, A.E. Ofomaja, Pseudo-second-order model for lead ion sorption from aqueous solutions onto palm kernel fiber, J. Hazard. Mat., 129 (2006) 137–142.
[32] T. Shahwan, Sorption kinetics: Obtaining a pseudo-second order rate equation based on a mass balance approach, J. Environ. Chem. Eng., 2 (2014) 1001–1006.
[33] R. Sawafta, T. Shahwan, A comparative study of the removal of methylene blue by iron nanoparticles from water and water-ethanol solutions, J. Mol. Liq., 273 (2019) 274–281.